
"Teaching Independent Parts Separately" (TIPSY-GAN) : Improving Accuracy and Stability in Unsupervised Adversarial 2D to 3D Pose Estimation

Peter Hardy*

Vision Learning and Control Research Group
University of Southampton
Hampshire, UK
p.t.d.hardy@soton.ac.uk

Srinandan Dasmahapatra

Vision Learning and Control Research Group
University of Southampton
Hampshire, UK
sd@ecs.soton.ac.uk

Hansung Kim

Vision Learning and Control Research Group
University of Southampton
Hampshire, UK
h.kim@soton.ac.uk

Abstract

We present TIPSY-GAN, a new approach to improve the accuracy and stability in unsupervised adversarial 2D to 3D human pose estimation. In our work we demonstrate that the human kinematic skeleton should not be assumed as a single spatially codependent structure; in fact, we posit when a full 2D pose is provided during training, there is an inherent bias learned where the 3D coordinate of a keypoint is spatially codependent on the 2D coordinates of all other keypoints. To investigate our hypothesis we follow previous adversarial approaches but train two generators on spatially independent parts of the kinematic skeleton, the torso and the legs. We find that improving the self-consistency cycle is key to lowering the evaluation error and therefore introduce new consistency constraints during training. A TIPSY model is produced via knowledge distillation from these generators which can predict the 3D ordinates for the entire 2D pose with improved results. Furthermore, we address an unanswered question in prior work of how long to train in a truly unsupervised scenario. We show that for two independent generators training adversarially has improved stability than that of a solo generator which collapses. TIPSY decreases the average error by 17% when compared to that of a baseline solo generator on the Human3.6M dataset. TIPSY improves upon other unsupervised approaches while also performing strongly against supervised and weakly-supervised approaches during evaluation on both the Human3.6M and MPI-INF-3DHP datasets. **Code and weights of our model will be made available**

1 Introduction

The ability to generate accurate 3D human skeletons from images and video has extensive applications in security, human-robot interaction, interactive media and healthcare [44, 9, 24]. Estimating a 3D pose from a single monocular image however, is an ill-posed inverse problem as multiple different 2D poses can correspond to the same 3D pose. Additionally, many state of the art 3D human pose

*<https://www.ecs.soton.ac.uk/people/ptdh1c20>

estimation (HPE) approaches [25, 5, 48, 15, 27, 23, 8, 33, 41, 51] utilise ground truth 3D pose data during training. Unfortunately most 3D datasets contain few subjects within a controlled environment and performing a limited number of actions. Unsupervised adversarial approaches [6, 18, 50] have sought to remedy this by exploiting the abundance of readily available 2D image and video data of humans. Through the use of self or temporal consistency and a 2D pose discriminator, they help to reduce the barrier of entry for 3D HPE while improving generability to unseen scenarios. However, most unsupervised approaches perform sub-par during evaluation on 3D HPE datasets when compared against their supervised counterparts. Our research aims to reduce this discrepancy and address what we believe is a flaw in all adversarial 2D to 3D HPE models; that the human kinematic skeleton should be treated as one independent structure.

We believe that minimising the predictive error on the entire 2D skeleton induces correlations between a keypoints 3D coordinate and all of the skeletons other 2D keypoint coordinates. Thus, for example, the 3D prediction for the left wrist would contain some component correlating to the 2D coordinate of the right knee. We instead train multiple generators on spatially independent parts of the 2D kinematic skeleton. The knowledge acquired is then distilled to an end-to-end model which can predict the 3D ordinates for an entire 2D pose, giving the framework its name "Teaching Independent Parts Separately" (TIPSY). In this paper we build upon Chen et al. [6] and show the stability of our model during training, highlighting that in a truly unsupervised scenario using spatially independent generators would allow for more optimum model to be created, even when no 3D data is accessible. Additionally we introduce three new self-consistency constraints during the adversarial learning cycle which we found to help improve evaluation metrics.

2 Related Work

2.1 3D Human Pose Estimation

There currently exist two main avenues of deep-learning research for 3D HPE. The first learns the mapping of 3D joints directly from a 2D image [31, 21, 26, 20, 37–39]. The second builds upon an accurate intermediate 2D pose estimate and learns how to lift a 3D pose from it. The 2D pose is obtained from an image through techniques such as Stacked-Hourglass Architectures [28] or Part Affinity Fields [4]. This work focuses on the latter 2D to 3D lifting avenue which can be organised into the following categories:

2.2 Fully Supervised

Fully supervised approaches seek to learn mappings from paired 2D-3D data which contain ground truth 2D locations of keypoints and their corresponding 3D coordinates. Martinez et al. [25] introduced a baseline fully connected regression model which learned 3D coordinates from their relative 2D locations. Exemplar approaches such as Chen and Ramanan [5] and Yang et al. [48] use large dictionaries/databases of 3D poses with a nearest-neighbour search to determine an optimal 3D pose. Jiang [15] introduced an exemplar approach that split their 3D dictionary into torso and legs aiming to speed up the nearest-neighbour search process, whereas we split up our poses during training to reduce bias and learn a better 3D mapping. Pavllo et al. [33] used temporal convolutions over 2D keypoints in order to predict the pose of the central or end frame in a time series, whereas Mehta et al. [27] utilised multi-task learning to combine a convolutional pose regressor with kinematic skeleton fitting for real time 3D pose estimation. Park and Kwak [30] and Zeng et al. [51] introduced the concept of splitting a pose into localised groups during learning, where they assume that an unseen pose may be composed of local joint configurations that appear in different poses within a training set. Unlike our approach however, Park and Kwak [30] and Zeng et al. [51] still maintain that an entire 2D pose is one independent structure via feature sharing or feature averaging between the localised groups throughout their network. We argue that no feature sharing is required and these localised groups can be assumed to be completely independent from one another. Additionally, we distill the knowledge from our sub-networks to an end-to-end network which is more computationally efficient and TIPSY has improved generalisation performance.

2.3 Weakly-Supervised

Weakly-Supervised approaches do not use explicit 2D-3D correspondences and instead use either augmented 3D data during training or unpaired 2D-3D data to learn human body priors (shape or articulation). Pavlakos et al. [32] and Ronchi et al. [35] proposed the learning of 3D poses from 2D with ordinal depth relationships between keypoints (e.g. the right wrist is behind the right elbow). Wandt and Rosenhahn [41] introduced a weakly-supervised adversarial approach which transformed their predicted and ground truth 3D poses into a kinematic chain [42] prior to being seen by a Wasserstein critic [11]. Yang et al. [49] lifted wild 2D poses where no ground truth data is available with a critic network that compared these against existing 3D skeletons. Zhou et al. [52] utilised transfer learning, using mixed 2D and 3D labels in a unified network. Drover et al. [7] investigated if 3D poses can be learned through 2D self-consistency alone, where they found a 2D pose critic network was also needed. We improve upon [7] within this work and show that self-consistency is more important than originally thought in order to minimise the quantitative error.

2.4 Unsupervised

Unsupervised approaches do not utilise any 3D data during training, unpaired or otherwise. Kudo et al. [18] introduced one of the first unsupervised adversarial networks utilising random re-projections and a 2D critic network, under the assumption that any predicted 3D pose once rotated and reprojected should still produce a believable 2D pose. Chen et al. [6] expanded this work and that of [7] by introducing an unsupervised adversarial approach with a self-consistency cycle. They also provided ablation studies highlighting a 7% improvement when using temporal cues during training. Yu et al. [50] built upon Chen et al. [6] highlighting that temporal constraints may hinder a models performance due to balancing multiple training objectives simultaneously and proposed splitting the problem into both a lifting and scale estimation module. They also found that adding temporal motion consistency can boost the performance of their model by 6%. Similar to [50] we highlight that another issue may lie within the lifting network which could also benefit from being split into two networks that predict upper and lower body keypoints.

2.5 Knowledge Distillation

Knowledge distillation is a model compression technique where knowledge is transferred from multiple or one large model (teacher) to a smaller model (student) [12]. Wang et al. [43] proposed distilling knowledge from a Non-Rigid Structure from Motion method based on exemplar learning to predict 3D poses. Weinzaepfel et al. [45] distilled knowledge from a 3D body, hand and facial pose estimators to a final model to predict the whole-body 3D pose. Their 3D body estimator however still assumed the entire body as one codependent structure during the training which we argue is sub-optimal. Additionally their model requires paired 2D-3D data during training whereas TIPSY achieves improved results when trained completely unsupervised. Tripathi et al. [40] investigated if knowledge could be distilled across 3D representations, where a teacher network would learn 3D kinematic skeletons from 2D poses, then distill this knowledge to a student network that would predict skinned multi-person linear model (SMPL) [22] representations of 3D poses. Lastly, Xu et al. [47] proposed an unsupervised approach where a self-consistent teacher with 2D pose-dictionary based modelling would distill knowledge to a student utilising graphical convolutions to improve estimation accuracy and flexibility. From our knowledge however, there is yet to be an approach that learns to predict 3D from spatially independent parts of a 2D pose and then distills this knowledge to an end-to-end model.

3 Method

In this section we describe both our adversarial approach to train our 2D to 3D generators, as well as our knowledge distillation approach for our final TIPSY model. Our 2D poses consist of N key-points (x_i, y_i) , $i = 1 \dots N$, with the root key-point, the midpoint between the left and right hip joint, being located at the origin $(0, 0)$. Because of the fundamental scale ambiguity associated with monocular images, it is impossible to infer absolute depth from a single view alone [29]. Therefore, we used max-normalisation on each of our 2D poses to scale their 2D coordinates between -1 and 1. This also constrains the range of possible 3D coordinates for these keypoints between -1 and 1, allowing the final function of our generators to be a bounded activation function which helps improve adversarial

learning [34]. Though feature selection [13, 46] can be used to find an optimal amount of spatially independent segments to split a 2D pose into, for simplicity we split our pose up into two during training, the torso and legs. Therefore, two generators will be trained using our adversarial approach and one final generator will be trained using knowledge distillation. The full end-to-end training process of our adversarial approach can be seen in Figure 1.

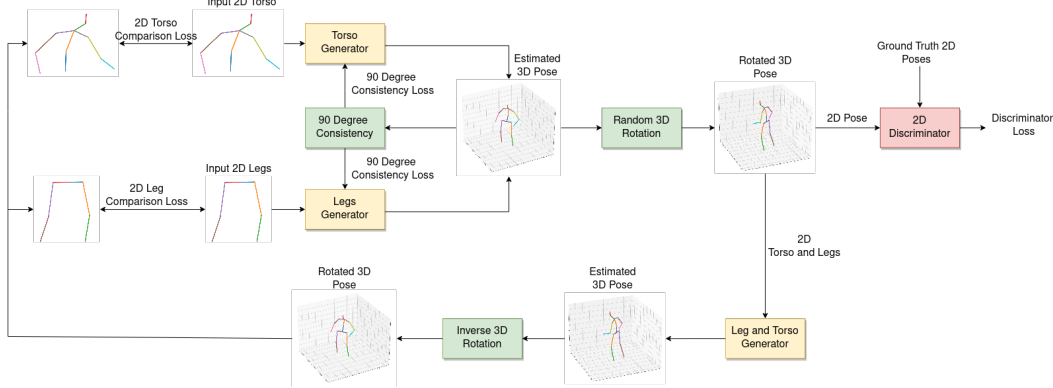


Figure 1: Adversarial learning process. A 2D pose is split into torso and legs and provided to their respective generator. The predicted 3D pose is randomly rotated and reprojected back into 2D and given to a discriminator. The 3D pose also goes through two forms of self-consistency, 90° and reprojection consistency.

3.1 Generator Architecture

Our generators (G_T, G_L) are fully connected neural networks whose architecture was based on Martinez et al. [25] and can be seen in Appendix A.1. These predict one 3D ordinate for each 2D keypoint:

$$G_T(\mathbf{x}_T, \mathbf{y}_T; \mathbf{w}_T) = \hat{\mathbf{z}}_T \quad G_L(\mathbf{x}_L, \mathbf{y}_L; \mathbf{w}_L) = \hat{\mathbf{z}}_L \quad (1)$$

where $(\mathbf{x}_T, \mathbf{y}_T)$ and $(\mathbf{x}_L, \mathbf{y}_L)$ are the 2D coordinates of all torso and leg keypoints respectively, $\hat{\mathbf{z}}_T$ and $\hat{\mathbf{z}}_L$ are the predicted 3D ordinate for those keypoints and \mathbf{w}_T and \mathbf{w}_L are the weights of each respective model learned during training. The torso generator takes a matrix as input containing the 2D coordinates for the wrists, elbows, shoulders, neck, spine, head and crown keypoint. The leg generator similarly accepts a matrix containing the ankles, knees and hips keypoints. The root keypoint being omitted during training as this was a constant. Once both of our generators had made their predictions they were concatenated with the original 2D keypoints to create our final predicted 3D pose $(\mathbf{x}, \mathbf{y}, \hat{\mathbf{z}})$. Our final TIPSY generator by contrast accepts the entire human poses keypoints as input and would predict the 3D ordinate for the full human pose.

3.2 Reprojection Consistency

Similar to prior work [6, 7, 50], we utilise a self-consistency cycle through random 3D rotations to reproject our predicted 3D poses to new synthetic 2D viewpoints. Let $\mathbf{Y} \in \mathbb{R}^{N \times 2}$ be our full 2D pose. This will be split into $\mathbf{Y}_T \in \mathbb{R}^{t \times 2}$ and $\mathbf{Y}_L \in \mathbb{R}^{l \times 2}$ containing the 2D keypoints from which our generators G_T, G_L will predict. Once a prediction $G_T(\mathbf{Y}_T), G_L(\mathbf{Y}_L)$ is made and a full 3D pose $(\mathbf{x}, \mathbf{y}, \hat{\mathbf{z}})$ obtained, a random rotation matrix \mathbf{R} will be created by uniformly sampling an azimuth angle between $[-\pi, \pi]$ and an elevation angle between $[-\frac{\pi}{18}, \frac{\pi}{18}]$. The predicted 3D pose will be rotated by this matrix and reprojected back to 2D via projection \mathbf{P} , obtaining a new synthetic viewpoint of the pose and the matrix $\tilde{\mathbf{Y}} \in \mathbb{R}^{N \times 2}$ where $\tilde{\mathbf{Y}} = \mathbf{P}\mathbf{R}[(\mathbf{x}, \mathbf{y}, \hat{\mathbf{z}})]$. Providing our model is consistent, if we now split $\tilde{\mathbf{Y}}$ into $\tilde{\mathbf{Y}}_T, \tilde{\mathbf{Y}}_L$ and provide these to our generators, perform the inverse rotation \mathbf{R}^{-1} on the newly predicted 3D pose $(\tilde{\mathbf{x}}, \tilde{\mathbf{y}}, \tilde{\mathbf{z}})$ and reproject it back into 2D, we should obtain our original matrix of 2D keypoints \mathbf{Y} . This cycle allows our generators to learn self-consistency

during training where they seek to minimise the following components in the loss function:

$$\mathcal{L}_{T2D} = \frac{1}{t} \|\mathbf{Y}_T - \mathbf{PR}^{-1}[(\tilde{\mathbf{x}}_T, \tilde{\mathbf{y}}_T, \tilde{\mathbf{z}}_T)]\|_F^2 \quad \mathcal{L}_{L2D} = \frac{1}{l} \|\mathbf{Y}_L - \mathbf{PR}^{-1}[(\tilde{\mathbf{x}}_L, \tilde{\mathbf{y}}_L, \tilde{\mathbf{z}}_L)]\|_F^2$$

Where $\|\cdot\|_F^2$ is squared frobenius norm and t and l are the number of keypoints predicted by the torso and leg generator respectively. Note that as we are training two generators independently from one another, they receive their own loss based on the error between the keypoints that they predicted for. As an example, part of the \mathcal{L}_{T2D} loss would include the difference between the original 2D keypoint location of the right wrist, and its 2D location once $(\tilde{\mathbf{x}}, \tilde{\mathbf{y}}, \tilde{\mathbf{z}})$ was inversely rotated and reprojected. This error would not be included in the \mathcal{L}_{L2D} loss as the leg generator does not predict the 3D location for this keypoint.

3.3 90 Degree Consistency

During our study we found that increasing self-consistency was key to reduce the evaluation error (see Appendix A.2. Therefore, we introduce new self-consistency constraints during training based on rotations around the y axis at 90° increments. Let $(\mathbf{x}, \mathbf{y}, \mathbf{z})$ be the predicted 3D pose from our model. If we assume a fixed camera position and rotate our pose 90° , then the depth component of our pose (\mathbf{z}) prior to rotation will now lie on the x axis from our cameras viewpoint. A visual example of this can be seen in Figure 2.

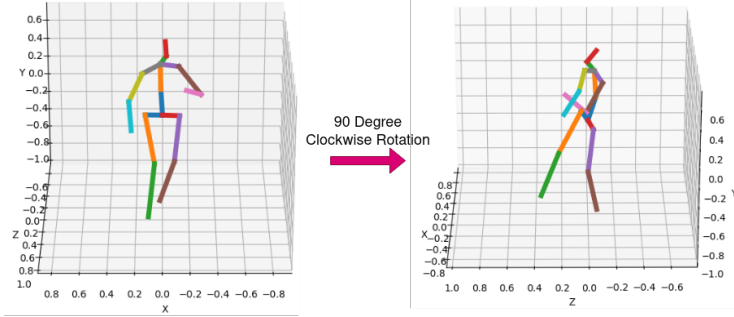


Figure 2: Showing that a 90° rotation of a 3D pose around the y axis with a fixed camera position, will result in the x axis values of the pose prior to rotation representing the z axis values of the pose after the rotation and vice versa.

As we have normalised the axis of our poses between -1 and 1, a 90° clockwise rotation of the 3D pose $(\mathbf{x}, \mathbf{y}, \mathbf{z})$ will produce the pose $(\mathbf{z}, \mathbf{y}, -\mathbf{x})$. Therefore, providing (\mathbf{z}, \mathbf{y}) as input to our generators should result in $-\mathbf{x}$ as its predictions. This fact allows for the inclusion of three additional consistency constraints in the loss function of our generators which teach consistency at a 90° clockwise rotation, a 90° anticlockwise rotation and a 180° rotation, which are as follows for the torso generator:

$$\frac{1}{t} [G_T(\mathbf{z}_T, \mathbf{y}_T; \mathbf{w}_T) + \mathbf{x}_T]^2 = 0 \quad (2)$$

$$\frac{1}{t} [G_T(-\mathbf{z}_T, \mathbf{y}_T; \mathbf{w}_T) - \mathbf{x}_T]^2 = 0 \quad (3)$$

$$\frac{1}{t} [G_T(\mathbf{x}_T, \mathbf{y}_T; \mathbf{w}_T) + G_T(-\mathbf{x}_T, \mathbf{y}_T; \mathbf{w}_T)]^2 = 0 \quad (4)$$

and equally defined for the leg generator. The left parts of these constraints are summed in the final loss function to produce \mathcal{L}_{T90° and \mathcal{L}_{L90° and given to their respective generator. Although we could include three similar constraints for 90° rotational increments around the x axis, we found that these hinder the performance of the model. This is due to 90° x axis rotations producing a birds eye and ground up view of a 2D pose, which contain little variation between their 2D keypoints.

3.4 Discriminator Loss

Although self-consistency is important, alone it is not a sufficient for generating realistic 3D skeletons [6]. Therefore, we utilise a 2D discriminator D , that takes as input a 2D pose and outputs a value between 0 and 1, representing the probability of the pose being plausible. The architecture of our discriminator is a fully connected neural network with the same structure as our generators, but containing one fewer residual blocks and a sigmoid function in place of Tanh. It learns to discriminate between the real 2D poses within our data \mathbf{Y} , and our reprojected 2D pose $\tilde{\mathbf{Y}}$. This provides feedback to the generators during training, enabling the learning of geometric priors such as joint angles and limb length ratios. Our discriminator D utilised the standard GAN loss [10]:

$$\min_G \max_D \mathcal{L}_{adv} = \mathbb{E}(\log(D(\mathbf{Y}))) + \mathbb{E}(\log(1 - D(\tilde{\mathbf{Y}}))) \quad (5)$$

Unlike the consistency constraints, we do not provide a unique version of L_{adv} to the torso and leg generator and instead provide the same loss (with a different weight) to both generators. This is due to two reasons. Firstly, we want our generators to produce a believable pose together which would in turn allow TIPSY to produce a believable pose by itself when knowledge was distilled. Having one discriminator see the entire 2D pose will provide this feedback during training. Secondly, we found that multiple discriminators would struggle to provide any useful feedback during training. An example being that 2D legs are normally represented as two straight or bent lines, making it hard for a discriminator to tell plausible and implausible poses apart.

3.5 Knowledge Distillation

The final step of our process, and the construction of our TIPSY model, is to distill the knowledge of our leg and torso generator to an end-to-end generator. This new generator G_{TIPSY} will accept the entire 2D pose as input and predict the 3D coordinates of the whole pose. G_{TIPSY} was trained to minimise the mean-squared error (MSE) between its own predictions and that of the leg and torso generator as shown:

$$\frac{1}{N} \|G_{TIPSY}(\mathbf{x}, \mathbf{y}) - \hat{\mathbf{z}}\|^2 \quad (6)$$

where $\hat{\mathbf{z}}$ is the 3D ordinates of all keypoints made by concatenating the leg and torso generators' predictions and N is the number of keypoints within the full human pose. We use MSE for knowledge distillation as we found training G_{TIPSY} adversarially, while including divergence from equation 6 as an additional constraint, lead to worse performance than matching the leg and torso generators' predictions.

3.6 Training

As discussed, our torso and leg generators were trained adversarially with rotational and 90° consistency and our TIPSY generator was trained using knowledge distillation. The network parameters are then updated to optimise the total loss for each generator given by:

$$\mathcal{L}_L = w_1 \mathcal{L}_{adv} + w_2 \mathcal{L}_{L2D} + w_3 \mathcal{L}_{L90^\circ} \quad (7)$$

$$\mathcal{L}_T = w_4 \mathcal{L}_{adv} + w_2 \mathcal{L}_{T2D} + w_3 \mathcal{L}_{T90^\circ} \quad (8)$$

$$\mathcal{L}_{TIPSY} = \frac{1}{N} \|G_{TIPSY}(\mathbf{x}, \mathbf{y}) - \hat{\mathbf{z}}\|^2 \quad (9)$$

where, $w_1 = 0.05$, $w_2 = 10$, $w_3 = 3$ and $w_4 = 0.08$ are the relative weights for the leg generators' adversarial loss, both generators' reprojection consistency loss, both generators' 90° consistency loss and torso generators' adversarial loss respectively. The discrepancy between w_1 and w_4 was due to how many keypoints each generator predicted. Our torso generator predicted 10 z coordinates out of 16 in the full pose. Meaning, they predicted $\frac{10}{16}$ of the entire pose. Therefore, any change in

adversarial loss would be more likely due to the torso generator than the leg generator and its weight is higher to reflect this. We trained our model completely unsupervised following Chen et al. [6] using a batch size of 8192 and the Adam optimiser [17] with a learning rate of 0.0002. Our experiments use $N = 16$ keypoints. During discriminator training we employ label flipping with a 5% chance.

4 Evaluation and Experiments

Here we compare and evaluate the performance of our TIPSY model against a baseline solo generator, our leg and torso generators and other state of the art models. Our results show that not only can our approach improve upon a baseline model, but it can also generalise well to unseen poses even when compared against more complex supervised and weakly-supervised approaches.

4.1 Quantitative Results On Human3.6M

Human3.6M [14] is one of the largest and most widely used 3D human pose datasets, containing 3.6 million 3D human poses. It consists of both video and motion capture (MoCap) data from 4 viewpoints of 5 female and 6 male subjects performing specific actions (e.g. talking on the phone, taking a photo, eating, etc.). There are two main evaluation protocols for the Human3.6M dataset, which use subjects 1, 5, 6, 7 and 8 for training and subject 9 and 11 for evaluation. Both protocols report the Mean Per Joint Position Error (MPJPE), which is the Euclidean distance in millimeters between the predicted and ground truth 3D coordinates. We report the protocol-II performance of our model which employs rigid alignment between the ground truth and predicted pose prior to evaluation. Our results can be seen in Table 1.

As we can see, by interpreting a 2D pose as multiple spatially independent sections for the purpose of 3D pose estimation, we can significantly improve results. This is highlighted by the 17% decrease in MPJPE between TIPSY and our baseline solo generator model. TIPSY also performed well against several fully supervised models and improved upon Chen et al. [6] which utilised temporal information. The three actions which saw the greatest improvement when using TIPSY over a baseline solo generator are Sitting, Walking and Directions. This is surprising for we would expect the legs and torsos during actions such as walking to share more co-dependence than the purchasing action however, our results seem to highlight the opposite.

4.2 Quantitative Results On MPI-INF-3DHP

MPI-INF-3DHP [26] is a markerless MoCap dataset containing the 3D human poses of 8 actors performing 8 different activities. To highlight the generability of TIPSY to unseen poses, we show the evaluation results on MPI-INF-3DHP when TIPSY is trained on Human3.6M. The evaluation metrics used are the *percentage of correctly positioned keypoints* (PCK3D) and *area under the curve* (AUC) as defined by Mehta et al. [26]. As our predicted poses are normalised, we scale them up by their original normalising factor prior to evaluation. Additionally Wandt and Rosenhahn [41] found there are ambiguities between multiple cameras and 3D pose rotations, causing the potential for inverted predictions as seen in Kudo et al. [18]. To remove this ambiguity we assume that the direction the person is facing with respect to the camera is known. Our results can be seen in Table 2.

Comparing TIPSY against Zeng et al. [51] we can see that although the PCK3D at a threshold of 150mm is similar, TIPSY has achieved an 11% improvement in AUC (threshold 0mm-150mm). This highlights that feature sharing between localised groups during training may dampen the generability of a model and that we may achieve improved results by treating them independently. Similarly TIPSY achieves a higher performance than other unsupervised and supervised approaches even when trained on the MPI-INF-3DHP dataset.

4.3 Adversarial Training Stability

One fundamental question when utilising unsupervised networks is when to stop training. However, we find a lack of information within prior work detailing how long authors have trained their models for. Therefore, we assume that prior work trained for a set amount of epochs and picked the weights across these epochs that performed best on an validation set. Though fine from an evaluation viewpoint, in practice this would not work if we had no ground truth data. In a truly unsupervised

Table 1: The reconstruction error (MPJPE) on Human3.6M. **Legend:** (+) denotes extra data — [49, 32] use 2D annotations from the MPII dataset, [7] increased the amount of Human3.6M training data by 8. (GT) denotes providing 2D ground truth keypoints to a lifting model. (T) denotes the use of temporal information. All comparison results are taking from their respective papers. Lower is better, best in bold, second best underlined.

Method	Approach	Direct.	Discuss	Eat	Greet	Phone	Photo	Posing	Purchase
Martinez et al. [25]	Supervised	39.5	43.2	46.4	47.0	51.0	56.0	41.4	40.6
Pavllo et al. [33] (GT)	Supervised	36.0	<u>38.7</u>	38.0	41.7	40.1	45.9	<u>37.1</u>	35.4
Cai et al. [3] (GT)	Supervised	36.8	<u>38.7</u>	38.2	41.7	40.7	46.8	<u>37.9</u>	35.6
Yang et al. [49] (+)	Weakly-Supervised	26.9	30.9	36.3	39.9	43.9	47.4	28.8	29.4
Pavlakos et al. [32] (+)	Weakly-Supervised	34.7	39.8	41.8	38.6	42.5	47.5	38.0	36.6
Ronchi et al. [35]	Weakly-Supervised	43.6	45.3	45.8	50.9	46.6	55.3	43.3	47.3
Wandt and Rosenhahn [41] (GT)	Weakly-Supervised	33.6	38.8	32.6	<u>37.5</u>	<u>36.0</u>	<u>44.1</u>	37.8	<u>34.9</u>
Drover et al. [7] (GT)(+)	Weakly-Supervised	<u>33.5</u>	39.3	<u>32.9</u>	37.0	35.8	42.7	39.0	<u>38.2</u>
Kudo et al. [18] (GT)	Unsupervised	125.0	137.9	107.2	130.8	115.1	127.3	147.7	128.7
Chen et al. [6] (T)	Unsupervised	-	-	-	-	-	-	-	-
Solo Generator (Ours)(GT)	Unsupervised	51.3	48.8	49.2	52.1	52.2	54.9	46.4	46.5
Leg and Torso Generator (Ours)(GT)	Unsupervised	39.3	40.2	38.7	45.7	43.1	53.1	40.1	41.5
TIPSY (Ours)(GT)	Knowledge Distillation	38.9	39.7	39.5	45.5	42.9	52.2	39.2	40.7
Method	Approach	Sit	SitD	Smoke	Wait	Walk	WalkD.	WalkT.	Avg.
Martinez et al. [25]	Supervised	56.5	69.4	49.2	45.0	49.5	38.0	43.1	47.7
Pavllo et al. [33] (GT)	Supervised	46.8	53.4	41.4	36.9	43.1	30.3	34.8	40.0
Cai et al. [3] (GT)	Supervised	47.6	51.7	41.3	36.8	42.7	<u>31.0</u>	34.7	40.2
Yang et al. [49] (+)	Weakly-Supervised	36.9	58.4	41.5	30.5	29.5	42.5	32.2	37.7
Pavlakos et al. [32] (+)	Weakly-Supervised	50.7	56.8	42.6	39.6	43.9	32.1	36.5	41.8
Ronchi et al. [35]	Weakly-Supervised	56.6	74.3	47.1	48.5	52.1	48.5	49.8	50.3
Wandt and Rosenhahn [41] (GT)	Weakly-Supervised	<u>39.2</u>	52.0	<u>37.5</u>	39.8	34.1	40.3	34.9	<u>38.2</u>
Drover et al. [7] (GT)(+)	Weakly-Supervised	42.1	52.3	36.9	39.4	36.8	33.2	34.9	<u>38.2</u>
Kudo et al. [18] (GT)	Unsupervised	134.7	139.8	114.5	147.1	130.8	125.6	151.1	130.9
Chen et al. [6] (GT)(T)	Unsupervised	-	-	-	-	-	-	-	51
Solo Generator (Ours)(GT)	Unsupervised	65.7	76.6	50.6	50.9	47.3	50.5	45.8	52.6
Leg and Torso Generator (Ours)(GT)	Unsupervised	51.3	62.4	42.9	39.7	36.4	46.6	40.6	44.1
TIPSY (Ours)(GT)	Knowledge Distillation	48.5	60.9	42.7	39.6	35.8	46.3	40.2	43.5

Table 2: Results on the MPI-INF-3DHP dataset. Our models are only trained on H36M **Legend:** (3DHP) denotes a model being trained on the MPI-INF-3DHP dataset. (H36M) denotes a model being trained on the Human3.6M dataset. (+) denotes additional training data. (*) uses transfer learning during from 2Dposenet. (T) denotes the use of temporal information during training. All comparison results are taking from their respective papers. Higher is better, best in bold, second best underlined.

Method	Approach	PCK3D	AUC
Mehta et al. [26] (3DHP + H36M)(*)	Supervised	76.5	40.8
Zeng et al. [51] (H36M)	Supervised	77.6	43.8
Yang et al. [49] (H36M)(+)	Weakly-Supervised	69.0	32.0
Wandt and Rosenhahn [41] (H36M)	Weakly-Supervised	81.8	54.8
Kanazawa et al. [16] (3DHP)	Weakly-Supervised	77.1	40.7
Chen et al. [6] (3DHP)(T)	Unsupervised	71.1	36.3
Kundu et al. [19] (H36M)	Unsupervised	76.5	39.8
Solo Generator (Ours)(H36M)	Unsupervised	75.7	47.0
Leg and Torso Generator (Ours)(H36M)	Unsupervised	77.1	47.9
TIPSY (Ours)(H36M)	Knowledge Distillation	<u>78.0</u>	48.8

scenario there are three approaches we could use to decide when to stop training. Firstly, we could monitor the discriminators loss and stop training when it too weak or strong. Though there is intuition for this approach, in practice a strong discriminator can cause a generator to fail due to vanishing gradients [1] and a weak discriminator provides poor feedback to a generator reducing its performance. Secondly, we could visualise the predictions per epoch and decide by eye which pose is the best. Though having potentially hundreds of epochs and thousands of poses, this is not an efficient solution. Lastly, and most realistically, we could pick the final weight during the training of our model or average the weights between a certain range of epochs to use. For this scenario we show the stability of 5 solo and 5 leg and torso generators during adversarial training which can be seen in Figure 3.

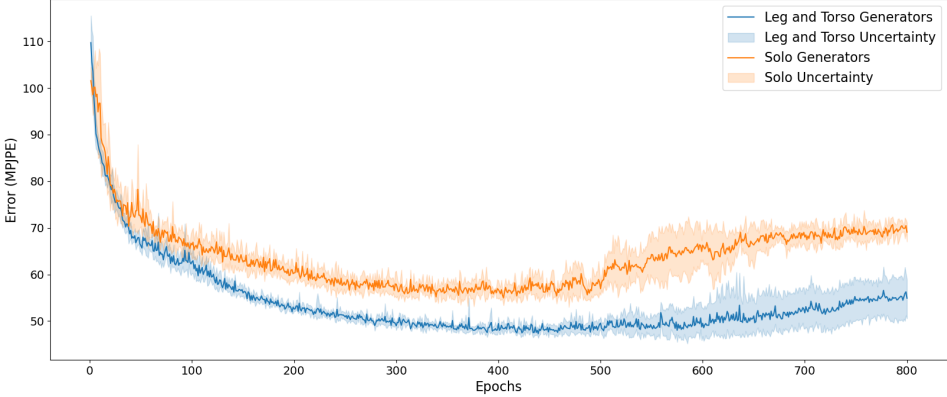


Figure 3: The evaluation error (MPJPE) of 5 leg and torso generators compared against 5 solo generators on the Human3.6M dataset for each training epoch. Note how the leg and torso generators error is more stable during learning where as the solo generators have more uncertainty.

As we can see, by having a leg and torso generator training independently not only is the MPJPE lower, but there is reduced uncertainty during the adversarial learning period (epochs 0-500). Our results also show that epoch 500 is where our discriminator learns the dataset, becoming too strong for both our models and causing a divergence away from the optimum. This is especially apparent within our solo generators' error as it diverged rapidly before settling around the 70mm mark. However, our leg and torso generators' error appears to slowly diverge from the optimum. There is a large uncertainty between our leg and torso generators' during this period however, so more comparisons are needed to see if this truly is the case. As these models were trained for 800 epochs. By choosing the last epochs weights to evaluate the average error of the leg and torso generators' would have been 54.9mm and our solo generators' average error would have been 68.9mm. If we had trained for 400 epochs then the average error of the leg and torso generators' would have been 48.0mm and the solo generators' 56.6mm. From epoch 300 to 600 the average error and standard deviation of our leg and torso generators' was 48.9 ± 2.2 mm, the average error and standard deviation of our solo generators' by comparison was 59.1 ± 4.2 mm. Going forward we would be interested to see if we are able to preempt the divergence observed from analysing changes within the loss of both our leg and torso generators and discriminator during training.

4.4 Are there still unintuitive keypoint correlations?

The motivation behind TIPSY came from the assumption that when we minimise the predictive error on the entire 2D skeleton, we induce correlations between a keypoints 3D prediction and all of other 2D keypoints, which we believed to be sub-optimal. Although we have shown that by learning independent segments we can achieve a 17% reduction in MPJPE, we are uncertain if this has also reduced correlations between keypoints that we would intuitively think of as independent. To investigate if these correlations have decreased, this section will explore the effect that changing a single keypoint has on the predictions of both a TIPSY model and a solo generator. With these results we can compare which prediction has changed most substantially and if this is what we as humans would intuitively think should change, i.e. we changed the left wrists 2D location therefore the left wrist and left elbow 3D prediction should change the most substantially. If however, the change in predictions is similar or negligible in both models, then we wish to understand why TIPSY has achieved such a substantial improvement.

To show how changing one specific 2D keypoint affects the 3D predictions of other keypoints within our model, we will show the squared difference in predictions once a selected keypoint has increased by 5% in size. As an example, if the 2D keypoint of the left wrist is (0.1, 0.1) and we wish to examine the affects it has on 3D prediction, then we will adjust its 2D coordinate to be (0.12, 0.12) while keeping all other 2D keypoints the same. The initial results of this study can be seen in Table 3, Table 4 and Table 5 which shows the squared difference in predictions due to increasing the right knees, left wrists and heads 2D coordinates respectively. Note for now that these are only the initial

results of this study and therefore only show the squared difference for a single pose. However, this still provides an insight into how one keypoint may influence each models overall predictions.

Keypoint	Solo Squared Difference ($\times 10^{-6}$)	TIPSY Squared Difference ($\times 10^{-6}$)
Right Hip	1.04	8.14
Right Knee	147.90	<u>130.20</u>
Right Ankle	571.30	297.30
Left Hip	7.09	4.81
Left Knee	3.69	3.05
Left Ankle	169.0	80.26
Spine	1.43	2.43
Neck	10.62	19.34
Head	34.40	7.26
Crown	104.80	4.65
Left Shoulder	20.28	0.06
Left Elbow	80.63	4.06
Left Wrist	75.24	0.45
Right Shoulder	7.31	0.07
Right Elbow	168.10	2.63
Right Wrist	<u>482.60</u>	22.27

Table 3: Showing the squared difference in z coordinate predictions of both our solo and TIPSY approach for each keypoint due to a 5% increase to the right knees 2D coordinate. Largest difference is in bold, second largest underlined

Examining Table 3, we can see the affect the right knees 2D coordinate has on the predictions of both models. This highlights that for the solo generator, any change in the 2D coordinate of the right knee mostly affects the 3D prediction for the right ankle. However, the second most influenced keypoint was that of the right wrist. Demonstrating that during adversarial learning, our solo generator has learned to correlate the right knees 2D coordinate and its 3D prediction for the right wrist. The results of our TIPSY model show a different story and go with human intuition, with the most influenced prediction being that of the right ankle followed by the right knee itself, which we assume would change most significantly as they are connected. Strangely however, the right wrist coordinate for our TIPSY model has the 4th largest difference. Meaning at some point during knowledge distillation, TIPSY also learned to somewhat correlate the right knees 2D coordinate with its 3D prediction for the right wrist. Though the difference is substantially smaller than that of the solo generator.

Table 4 paints a similar picture to before, where TIPSY has managed to learn correlations between 2D coordinates and their own 3D predictions, as well the predictions of connected keypoints within the human pose. This is shown by the biggest difference in predictions being that of the left wrist followed by the left elbow. Our solo generator however has barely adjusted its prediction for the left elbow and in fact adjusted its prediction for the right wrist the most. This goes against our own intuition as we are able to easily move our left and right wrist independently from one another. Similarly, our solo generator has adjusted its predictions for the crown and left ankle keypoint. These again are keypoints we would assume to be independent from the left wrist.

Surprisingly Table 5 shows that TIPSY has induced correlations between keypoints that we would not expect. As changing the 2D location of the head has resulted in the right wrists 3D prediction seeing the biggest change, followed by the crown. The solo generator also had similar results with the biggest difference being observed in the crowns prediction and then the right wrist. It is worth noting however that TIPSY has fewer unintuitive correlations, such as the right ankle difference being quite high within the solo generator, but low in the TIPSY model. This shows that in this circumstance TIPSY has induced a correlation we would not expect, overall the unintuitive correlations between keypoints has been reduced.

Keypoint	Solo Squared Difference ($\times 10^{-6}$)	TIPSY Squared Difference ($\times 10^{-6}$)
Right Hip	8.39	0.54
Right Knee	0.15	0.47
Right Ankle	6.32	15.04
Left Hip	7.77	1.03
Left Knee	0.16	2.36
Left Ankle	81.94	2.14
Spine	7.81	2.16
Neck	7.65	25.2
Head	48.84	7.21
Crown	138.43	12.02
Left Shoulder	35.29	8.94
Left Elbow	1.01	<u>563.39</u>
Left Wrist	<u>372.19</u>	1651.88
Right Shoulder	<u>17.45</u>	0.79
Right Elbow	35.95	11.01
Right Wrist	525.75	87.84

Table 4: Showing the squared difference in z coordinate predictions of both our solo and TIPSY approach for each keypoint due to a 5% increase to the left wrists 2D coordinate. Largest difference is in bold, second largest underlined

Keypoint	Solo Squared Difference ($\times 10^{-6}$)	TIPSY Squared Difference ($\times 10^{-6}$)
Right Hip	0.02	3.70
Right Knee	24.04	4.59
Right Ankle	183.73	4.42
Left Hip	0.02	2.03
Left Knee	32.70	3.30
Left Ankle	19.68	3.75
Spine	7.79	0.01
Neck	36.28	45.84
Head	68.46	89.20
Crown	406.19	<u>170.68</u>
Left Shoulder	29.15	<u>65.23</u>
Left Elbow	54.10	21.84
Left Wrist	161.46	1.99
Right Shoulder	9.27	42.98
Right Elbow	111.85	41.26
Right Wrist	398.49	288.77

Table 5: Showing the squared difference in z coordinate predictions of both our solo and TIPSY approach for each keypoint due to a 5% increase to the heads 2D coordinate. Largest difference is in bold, second largest underlined

5 Conclusions

This paper presented TIPSY, an improved unsupervised training approach for 3D human pose estimation which learns how to lift independent segments of the 2D kinematic skeleton separately. Our approach introduces new additional consistency constraints which improve the adversarial self-consistency cycle and lower the quantitative error. Moreover, we highlighted that in a truly unsupervised scenario TIPSY would allow for an optimum model to be created through increased GAN stability. In fact, by exploiting the spatial independence of the torso and legs we are able to reduce the evaluation error by 17% and comparing well against supervised and weakly-supervised approaches on the Human3.6M dataset. Furthermore, we believe that a TIPSY training approach could be used to help improve the performance of both supervised and weakly-supervised approaches. Additionally, our high AUC performance in the MPI-INF-3DHP dataset with a model trained on H36M demonstrates that a TIPSY approach can generalise well to unseen poses, improving upon prior supervised models that assume a 2D pose should be treated as codependent localised groups. From

our initial analysis we can see that these results may be due to the correlations between independent keypoints being reduced. However, this still requires further investigation as we have so far only investigated the affect of a few keypoints on one pose.

References

- [1] Martín Arjovsky and Léon Bottou. Towards principled methods for training generative adversarial networks. *ArXiv*, abs/1701.04862, 2017.
- [2] Jimmy Lei Ba, Jamie Ryan Kiros, and Geoffrey E. Hinton. Layer normalization, 2016. URL <https://arxiv.org/abs/1607.06450>.
- [3] Yujun Cai, Liuhan Ge, Jun Liu, Jianfei Cai, Tat-Jen Cham, Junsong Yuan, and Nadia Magnenat Thalmann. Exploiting spatial-temporal relationships for 3d pose estimation via graph convolutional networks. In *2019 IEEE/CVF International Conference on Computer Vision (ICCV)*, pages 2272–2281, 2019. doi: 10.1109/ICCV.2019.00236.
- [4] Z. Cao, G. Hidalgo, T. Simon, S. Wei, and Y. Sheikh. Openpose: Realtime multi-person 2d pose estimation using part affinity fields. *IEEE Transactions on Pattern Analysis and Machine Intelligence*, 43(01):172–186, jan 2021. ISSN 1939-3539. doi: 10.1109/TPAMI.2019.2929257.
- [5] Ching-Hang Chen and Deva Ramanan. 3d human pose estimation = 2d pose estimation + matching. *2017 IEEE Conference on Computer Vision and Pattern Recognition (CVPR)*, pages 5759–5767, 2017.
- [6] Ching-Hang Chen, Ambrish Tyagi, Amit Agrawal, Dylan Drover, M. V. Rohith, Stefan Stoianov, and James M. Rehg. Unsupervised 3d pose estimation with geometric self-supervision. *2019 IEEE/CVF Conference on Computer Vision and Pattern Recognition (CVPR)*, pages 5707–5717, 2019.
- [7] Dylan Drover, Rohith M. V, Ching-Hang Chen, Amit Agrawal, Ambrish Tyagi, and Cong Phuoc Huynh. Can 3d pose be learned from 2d projections alone? In Laura Leal-Taixé and Stefan Roth, editors, *Computer Vision – ECCV 2018 Workshops*, pages 78–94, Cham, 2019. Springer International Publishing. ISBN 978-3-030-11018-5.
- [8] Haoshu Fang, Yuanlu Xu, Wenguan Wang, Xiaobai Liu, and Song-Chun Zhu. Learning pose grammar to encode human body configuration for 3d pose estimation. In *AAAI*, 2018.
- [9] David A Forsyth, Okan Arikan, Leslie Ikemoto, Deva Ramanan, and James O’Brien. Computational studies of human motion: Tracking and motion synthesis. 2006.
- [10] Ian Goodfellow, Jean Pouget-Abadie, Mehdi Mirza, Bing Xu, David Warde-Farley, Sherjil Ozair, Aaron Courville, and Yoshua Bengio. Generative adversarial nets. In Z. Ghahramani, M. Welling, C. Cortes, N. Lawrence, and K. Q. Weinberger, editors, *Advances in Neural Information Processing Systems*, volume 27. Curran Associates, Inc., 2014. URL <https://proceedings.neurips.cc/paper/2014/file/5ca3e9b122f61f8f06494c97b1afccf3-Paper.pdf>.
- [11] Ishaan Gulrajani, Faruk Ahmed, Martin Arjovsky, Vincent Dumoulin, and Aaron C Courville. Improved training of wasserstein gans. In I. Guyon, U. V. Luxburg, S. Bengio, H. Wallach, R. Fergus, S. Vishwanathan, and R. Garnett, editors, *Advances in Neural Information Processing Systems*, volume 30. Curran Associates, Inc., 2017. URL <https://proceedings.neurips.cc/paper/2017/file/892c3b1c6dccc52936e27cbd0ff683d6-Paper.pdf>.
- [12] Geoffrey E. Hinton, Oriol Vinyals, and Jeffrey Dean. Distilling the knowledge in a neural network. *ArXiv*, abs/1503.02531, 2015.
- [13] Yingkun Huang, Weidong Jin, Zhibin Yu, and Bing Li. Supervised feature selection through deep neural networks with pairwise connected structure. *Knowledge-Based Systems*, 204:106202, 07 2020. doi: 10.1016/j.knosys.2020.106202.
- [14] Catalin Ionescu, Dragos Papava, Vlad Olaru, and Cristian Sminchisescu. Human3.6m: Large scale datasets and predictive methods for 3d human sensing in natural environments. *IEEE Transactions on Pattern Analysis and Machine Intelligence*, 36(7):1325–1339, jul 2014.

[15] Hao Jiang. 3d human pose reconstruction using millions of exemplars. In *2010 20th International Conference on Pattern Recognition*, pages 1674–1677, 2010. doi: 10.1109/ICPR.2010.414.

[16] Angjoo Kanazawa, Michael J. Black, David W. Jacobs, and Jitendra Malik. End-to-end recovery of human shape and pose. In *2018 IEEE/CVF Conference on Computer Vision and Pattern Recognition*, pages 7122–7131, 2018. doi: 10.1109/CVPR.2018.00744.

[17] Diederik P. Kingma and Jimmy Ba. Adam: A method for stochastic optimization. *CoRR*, abs/1412.6980, 2015.

[18] Yasunori Kudo, Keisuke Ogaki, Yusuke Matsui, and Yuri Odagiri. Unsupervised adversarial learning of 3d human pose from 2d joint locations, 2018.

[19] Jogendra Nath Kundu, Siddharth Seth, Mayur Rahul, M. Rakesh, Venkatesh Babu Radhakrishnan, and Anirban Chakraborty. Kinematic-structure-preserved representation for unsupervised 3d human pose estimation. In *AAAI*, 2020.

[20] Sijin Li, Weichen Zhang, and Antoni B. Chan. Maximum-margin structured learning with deep networks for 3d human pose estimation. *International Journal of Computer Vision*, 122: 149–168, 2015.

[21] Wen-Nung Lie, Guan-Han Lin, Lung-Sheng Shih, Yuling Hsu, Thang Huu Nguyen, and Quynh Nguyen Quang Nhu. Fully convolutional network for 3d human skeleton estimation from a single view for action analysis. In *2019 IEEE International Conference on Multimedia Expo Workshops (ICMEW)*, pages 1–6, 2019. doi: 10.1109/ICMEW.2019.0-120.

[22] Matthew Loper, Naureen Mahmood, Javier Romero, Gerard Pons-Moll, and Michael J. Black. SMPL: A skinned multi-person linear model. *ACM Trans. Graphics (Proc. SIGGRAPH Asia)*, 34(6):248:1–248:16, October 2015.

[23] Chenxu Luo, Xiao Chu, and Alan Loddon Yuille. Orinet: A fully convolutional network for 3d human pose estimation. *ArXiv*, abs/1811.04989, 2018.

[24] D. Luvizon, H. Tabia, and David Picard. Multi-task deep learning for real-time 3d human pose estimation and action recognition. *IEEE transactions on pattern analysis and machine intelligence*, 2020.

[25] Julieta Martinez, Mir Rayat Imtiaz Hossain, Javier Romero, and J.J. Little. A simple yet effective baseline for 3d human pose estimation. pages 2659–2668, 10 2017. doi: 10.1109/ICCV.2017.288.

[26] Dushyant Mehta, Helge Rhodin, Dan Casas, Pascal Fua, Oleksandr Sotnychenko, Weipeng Xu, and Christian Theobalt. Monocular 3d human pose estimation in the wild using improved cnn supervision. In *3D Vision (3DV), 2017 Fifth International Conference on*. IEEE, 2017. doi: 10.1109/3dv.2017.00064. URL http://gvv.mpi-inf.mpg.de/3dhp_dataset.

[27] Dushyant Mehta, Srinath Sridhar, Oleksandr Sotnychenko, Helge Rhodin, Mohammad Shafiei, Hans-Peter Seidel, Weipeng Xu, Dan Casas, and Christian Theobalt. Vnect: Real-time 3d human pose estimation with a single rgb camera. volume 36, 2017. doi: 10.1145/3072959.3073596. URL <http://gvv.mpi-inf.mpg.de/projects/VNect/>.

[28] Alejandro Newell, Kaiyu Yang, and Jia Deng. Stacked hourglass networks for human pose estimation. In Bastian Leibe, Jiri Matas, Nicu Sebe, and Max Welling, editors, *Computer Vision – ECCV 2016*, pages 483–499, Cham, 2016. Springer International Publishing. ISBN 978-3-319-46484-8.

[29] Mark Nishimura, David B. Lindell, Christopher Metzler, and Gordon Wetzstein. Disambiguating monocular depth estimation with a single transient. In Andrea Vedaldi, Horst Bischof, Thomas Brox, and Jan-Michael Frahm, editors, *Computer Vision – ECCV 2020*, pages 139–155, Cham, 2020. Springer International Publishing. ISBN 978-3-030-58589-1.

[30] Sungheon Park and Nojun Kwak. 3d human pose estimation with relational networks. In *BMVC*, 2018.

[31] Georgios Pavlakos, Xiaowei Zhou, Konstantinos G. Derpanis, and Kostas Daniilidis. Coarse-to-fine volumetric prediction for single-image 3d human pose. *2017 IEEE Conference on Computer Vision and Pattern Recognition (CVPR)*, pages 1263–1272, 2017.

[32] Georgios Pavlakos, Xiaowei Zhou, and Kostas Daniilidis. Ordinal depth supervision for 3d human pose estimation. pages 7307–7316, 06 2018. doi: 10.1109/CVPR.2018.00763.

[33] Dario Pavllo, Christoph Feichtenhofer, David Grangier, and Michael Auli. 3d human pose estimation in video with temporal convolutions and semi-supervised training. pages 7745–7754, 06 2019. doi: 10.1109/CVPR.2019.00794.

[34] Alec Radford, Luke Metz, and Soumith Chintala. Unsupervised representation learning with deep convolutional generative adversarial networks. *CoRR*, abs/1511.06434, 2016.

[35] Matteo Ruggero Ronchi, Oisin Mac Aodha, Robert Eng, and Pietro Perona. It’s all relative: Monocular 3d human pose estimation from weakly supervised data. In *British Machine Vision Conference 2018, BMVC 2018, Northumbria University, Newcastle, UK, September 3-6, 2018*, page 300, 2018. URL <http://bmvc2018.org/contents/papers/0182.pdf>.

[36] Shibani Santurkar, Dimitris Tsipras, Andrew Ilyas, and Aleksander Madry. How does batch normalization help optimization? In S. Bengio, H. Wallach, H. Larochelle, K. Grauman, N. Cesa-Bianchi, and R. Garnett, editors, *Advances in Neural Information Processing Systems*, volume 31. Curran Associates, Inc., 2018. URL <https://proceedings.neurips.cc/paper/2018/file/905056c1ac1dad141560467e0a99e1cf-Paper.pdf>.

[37] X. Sun, J. Shang, S. Liang, and Y. Wei. Compositional human pose regression. In *2017 IEEE International Conference on Computer Vision (ICCV)*, pages 2621–2630, Los Alamitos, CA, USA, oct 2017. IEEE Computer Society. doi: 10.1109/ICCV.2017.284. URL <https://doi.ieee.org/10.1109/ICCV.2017.284>.

[38] Bugra Tekin, Isinsu Katircioglu, Mathieu Salzmann, Vincent Lepetit, and Pascal Fua. Structured prediction of 3d human pose with deep neural networks. In Edwin R. Hancock Richard C. Wilson and William A. P. Smith, editors, *Proceedings of the British Machine Vision Conference (BMVC)*, pages 130.1–130.11. BMVA Press, September 2016. ISBN 1-901725-59-6. doi: 10.5244/C.30.130. URL <https://dx.doi.org/10.5244/C.30.130>.

[39] D Tome, Christopher Russell, and L Agapito. Lifting from the deep: Convolutional 3d pose estimation from a single image, 2017.

[40] S. Tripathi, S. Ranade, A. Tyagi, and A. Agrawal. Posenet3d: Learning temporally consistent 3d human pose via knowledge distillation. In *2020 International Conference on 3D Vision (3DV)*, pages 311–321, Los Alamitos, CA, USA, nov 2020. IEEE Computer Society. doi: 10.1109/3DV50981.2020.00041. URL <https://doi.ieee.org/10.1109/3DV50981.2020.00041>.

[41] Bastian Wandt and Bodo Rosenhahn. Repnet: Weakly supervised training of an adversarial reprojection network for 3d human pose estimation. In *2019 IEEE/CVF Conference on Computer Vision and Pattern Recognition (CVPR)*, pages 7774–7783, 2019. doi: 10.1109/CVPR.2019.00797.

[42] Bastian Wandt, Hanno Ackermann, and Bodo Rosenhahn. A kinematic chain space for monocular motion capture. In *ECCV Workshops*, 2018.

[43] Chaoyang Wang, Chen Kong, and Simon Lucey. Distill knowledge from nrsfm for weakly supervised 3d pose learning. *2019 IEEE/CVF International Conference on Computer Vision (ICCV)*, pages 743–752, 2019.

[44] Jinbao Wang, Shujie Tan, Xiantong Zhen, Shuo Xu, Feng Zheng, Zhenyu He, and Ling Shao. Deep 3d human pose estimation: A review. *Computer Vision and Image Understanding*, 210:103225, 2021. ISSN 1077-3142. doi: <https://doi.org/10.1016/j.cviu.2021.103225>. URL <https://www.sciencedirect.com/science/article/pii/S1077314221000692>.

[45] Philippe Weinzaepfel, Romain Brégier, Hadrien Combaluzier, Vincent Leroy, and Grégory Rogez. Dope: Distillation of part experts for whole-body 3d pose estimation in the wild. In *Computer Vision – ECCV 2020: 16th European Conference, Glasgow, UK, August 23–28, 2020, Proceedings, Part XXVI*, page 380–397, Berlin, Heidelberg, 2020. Springer-Verlag. ISBN 978-3-030-58573-0. doi: 10.1007/978-3-030-58574-7_23. URL https://doi.org/10.1007/978-3-030-58574-7_23.

[46] Maksymilian Wojtas and Ke Chen. Feature importance ranking for deep learning. In *Advances in Neural Information Processing Systems 33*, Advances in Neural Information Processing Systems. Morgan Kaufmann Publishers, September 2020. 34th Conference on Neural Information Processing Systems, NeurIPS 2020 ; Conference date: 06-12-2020 Through 12-12-2020.

[47] Chenxin Xu, Siheng Chen, Maosen Li, and Ya Zhang. Invariant teacher and equivariant student for unsupervised 3d human pose estimation. In *Proceedings of the AAAI Conference on Artificial Intelligence*, volume 35, pages 3013–3021, 2021.

[48] Jingjing Yang, Lili Wan, Wanru Xu, and Shenghui Wang. 3d human pose estimation from a single image via exemplar augmentation. *Journal of Visual Communication and Image Representation*, 59:371–379, 2019. ISSN 1047-3203. doi: <https://doi.org/10.1016/j.jvcir.2019.01.033>. URL <https://www.sciencedirect.com/science/article/pii/S1047320319300446>.

[49] Wei Yang, Wanli Ouyang, X. Wang, Jimmy S. J. Ren, Hongsheng Li, and Xiaogang Wang. 3d human pose estimation in the wild by adversarial learning. *2018 IEEE/CVF Conference on Computer Vision and Pattern Recognition*, pages 5255–5264, 2018.

[50] Zhenbo Yu, Bingbing Ni, Jingwei Xu, Junjie Wang, Chenglong Zhao, and Wenjun Zhang. Towards alleviating the modeling ambiguity of unsupervised monocular 3d human pose estimation. In *Proceedings of the IEEE/CVF International Conference on Computer Vision (ICCV)*, pages 8651–8660, October 2021.

[51] Ailing Zeng, Xiao Sun, Fuyang Huang, Minhao Liu, Qiang Xu, and Stephen Lin. Srnet: Improving generalization in 3d human pose estimation with a split-and-recombine approach. In Andrea Vedaldi, Horst Bischof, Thomas Brox, and Jan-Michael Frahm, editors, *Computer Vision – ECCV 2020*, pages 507–523, Cham, 2020. Springer International Publishing. ISBN 978-3-030-58568-6.

[52] Xingyi Zhou, Qixing Huang, Xiao Sun, Xiangyang Xue, and Yichen Wei. Towards 3d human pose estimation in the wild: A weakly-supervised approach. In *The IEEE International Conference on Computer Vision (ICCV)*, Oct 2017.

A Appendix

A.1 Additional Figures

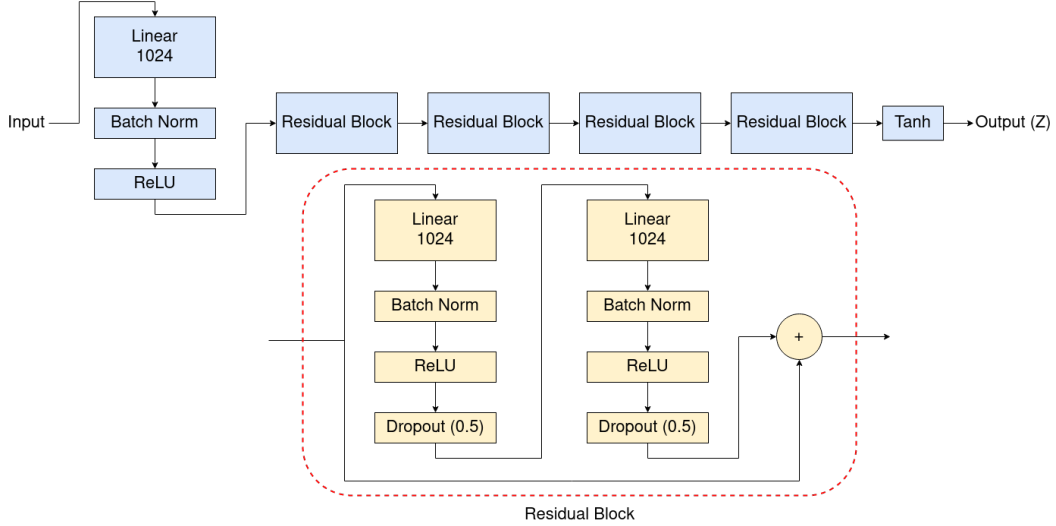


Figure 4: Generator architecture. The network consists of one linear, batch normalisation and activation layer followed by 4 residual blocks. A hyperbolic tangent function would then predict the Z values between -1 and 1. The discriminator is has one fewer residual block and sigmoid in place of Tanh.

A.2 Improving the consistency cycle

We found during our study that we are able to achieve a better quantitative error by improving self-consistency even if this leads to a pose that is easy to discriminate against. This can be seen clearly in Table 6 where we see a noticeable decrease in MPJPE between the results in Drover et al. [7] and our re-creation with the additional consistency constraints mentioned within our work.

Model	Avg.
Drover <i>et al.</i> [7]	38.2
Ours (Improved Consistency)	34.9

Table 6: The results of Drover et al. [7] and our recreation with our additional consistency constraints and changing the weight values of the loss function to increase the importance of self-consistency.

Because of this, we sought to replace the random rotation self-consistency cycle with something more efficient. This was due to a random rotation lending itself to long training times, where the longer a model is trained the more random rotations it will see and therefore the more consistent it will become. However, this could be a problem as highlighted in Figure 3 where a longer training period may lead to GAN instability. By contrast our 90° consistency constraints allows for 3 specified angles of consistency to be learned per training iteration, while also being more computational efficient than randomly rotation a 3D object and re-projecting it. These by themselves however aren't sufficient to learn self-consistency as the model only learns 3 specific angles during training and in the wild many more viewpoints exist. We therefore sought an optimisation formula similar to our 90° consistency that would satisfy all possible viewpoints around the y axis. First let us determine the end position of the pose $(\mathbf{x}, \mathbf{y}, \hat{\mathbf{z}}_i)$ after a random 3D rotation \mathbf{R}_θ along the y axis:

$$\begin{aligned}
\mathbf{R}_\theta &= \begin{bmatrix} \cos(\theta) & 0 & -\sin(\theta) \\ 0 & 1 & 0 \\ \sin(\theta) & 0 & \cos(\theta) \end{bmatrix} \\
\mathbf{R}_\theta \begin{bmatrix} \mathbf{x} \\ \mathbf{y} \\ \hat{\mathbf{z}} \end{bmatrix} &= \begin{bmatrix} \mathbf{x}\cos(\theta) - \hat{\mathbf{z}}\sin(\theta) \\ \mathbf{y} \\ \mathbf{x}\sin(\theta) + \hat{\mathbf{z}}\cos(\theta) \end{bmatrix}
\end{aligned} \tag{10}$$

we substitute these new positions within our generator function:

$$\mathbf{x}\sin(\theta) + \hat{\mathbf{z}}\cos(\theta) = G(\mathbf{x}\cos(\theta) - \hat{\mathbf{z}}\sin(\theta), \mathbf{y}; \mathbf{w}) \tag{11}$$

for $\theta \ll 1$:

$$\mathbf{x}\theta + \hat{\mathbf{z}} = G(\mathbf{x} - \mathbf{z}\theta, \mathbf{y}; \mathbf{w}) \tag{12}$$

perform Taylor series expansion while ignoring terms of power 2 and above for the small angle θ :

$$\mathbf{x}\theta + \hat{\mathbf{z}} = G(\mathbf{x}, \mathbf{y}; \mathbf{w}) - \hat{\mathbf{z}}\theta \frac{\partial}{\partial \mathbf{x}} G(\mathbf{x}, \mathbf{y}; \mathbf{w}) \tag{13}$$

cancel \mathbf{z} with $G(\mathbf{x}, \mathbf{y}; \mathbf{w})$ and remove θ :

$$\mathbf{x} = -\hat{\mathbf{z}} \frac{\partial}{\partial \mathbf{x}} G(\mathbf{x}, \mathbf{y}; \mathbf{w}) \tag{14}$$

this leaves us with our final consistency constraint for all angles:

$$\mathbf{x} + \hat{\mathbf{z}} \frac{\partial}{\partial \mathbf{x}} G(\mathbf{x}, \mathbf{y}; \mathbf{w}) = 0 \tag{15}$$

Although theoretically simple, in practice the above is difficult to implement and leads to lackluster performance. This is due to two factors; firstly the derivative component is a Jacobian matrix, which to calculate numerically within current deep learning languages is computationally inefficient, requiring over 100 minutes to train one epoch on an RTX-8000 GPU. Secondly as we are finding the derivative with respect to the inputs, to maintain gradient independence all batch-norm layers have to be removed from our model as these normalises across the batch dimension. This has the effect of lowering the rate at which our model learns and decreasing its stability while training [36]. We are currently investigating if layer norm [2] would be a suitable replacement for batch norm as this would retain gradient independence and allow the implementation of the above within future work.